Characterization of Task-Free/Task-Performance Brain States

Xin Zhang[1,2], Lei Guo[1], Xiang Li[2], Dajiang Zhu[2], Kaiming Li[3], Zhenqiang Sun[4], Changfeng Jin[5], Xintao Hu[1], Junwei Han[1], Qun Zhao[6], Lingjiang Li[5], and Tianming Liu[2]

[1] School of Automation, Northwestern Polytechnical University, Xi'an, China
[2] Department of Computer Science and Bioimaging Research Center, The University of Georgia, Athens, GA
[3] Biomedical Imaging Technology Center, Emory University, Atlanta, GA
[4] The School of Electronic and Information Engineering, Xi'an Jiaotong University, Xi'an, China
[5] The Mental Health Institute, The Second Xiangya Hospital, Central South University, Changsha, China
[6] Department of Physics and Astronomy and Bioimaging Research Center, The University of Georgia, Athens, GA

Abstract. Both resting state fMRI (R-fMRI) and task-based fMRI (T-fMRI) have been widely used to study the functional activities of the human brain during task-free and task-performance periods, respectively. However, due to the difficulty in strictly controlling the participating subject's mental status and their cognitive behaviors during fMRI scans, it has been very challenging to tell whether or not an R-fMRI/T-fMRI scan truly reflects the participant's functional brain states in task-free/task-performance. This paper presents a novel approach to characterizing the brain's functional status into task-free or task-performance states. The basic idea here is that the brain's functional state is represented by a whole-brain quasi-stable connectivity pattern (WQCP), and an effective sparse coding procedure was then applied to learn the atomic connectivity patterns (ACP) of both task-free and task-performance states based on training R-fMRI and T-fMRI data. Our experimental results demonstrated that the learned ACPs for R-fMRI and T-fMRI datasets are substantially different, as expected. However, a certain portion of ACPs from R-fMRI and T-fMRI datasets are overlapping, suggesting that those subjects with overlapping ACPs were not in the expected task-free/task-performance states during R-fMRI/T-fMRI scans.

Keywords: DTI, fMRI, connectivity, cortical landmarks.

1 Introduction

In the brain imaging field, resting state fMRI (R-fMRI) [1, 2] and task-based fMRI (T-fMRI) [3] have been widely employed to investigate the functional activities of the human brain in task-free and task-performance periods. However, it has been rarely

N. Ayache et al. (Eds.): MICCAI 2012, Part II, LNCS 7511, pp. 237–245, 2012.

studied (as far as we know) whether or not the R-fMRI/T-fMRI data was really reflecting the subject's task-free/task-performance states, in that it is very difficult to strictly control the participating subject's mental status and their cognitive behaviors during fMRI scan sessions. For instance, if a participating subject's brain was active, e.g., in some active cognitive processes, during the R-fMRI scan, how different will this R-fMRI data be from other strict R-fMRI data acquired during task-free states? Similarly, if a participating subject's brain was in resting state, e.g. not strictly following the administered task-performance paradigm [10], how different will this T-fMRI data be from other strict T-fMRI data scanned during task-performance states? If these differences are substantial, can we quantitatively characterize and automatically differentiate those unreliable or false R-fMRI/T-fMRI data from strict R-fMRI/T-fMRI data? The answers and solutions to these questions can significantly enhance our understanding of the function mechanisms of the brain and enable us to detect and control the quality of R-fMRI/T-fMRI data in the subsequent quantitative analysis, e.g., inference of resting state networks (RSNs), functional connectivity analysis, and task-based functional region localization.

In response to the above unanswered questions, this paper presents a novel computational framework to characterize the brain's task-free and task-performance functional states by learning from both R-fMRI and T-fMRI datasets. The basic idea is that we represent the brain's functional status by whole-brain quasi-stable connectivity patterns (WQCP), and then apply a sparse coding approach to learn the atomic connectivity patterns (ACP) of both task-free and task-performance states from large-scale temporally segmented WQCPs. Notably, the integration and pooling of many WQCPs from different brains are enabled by our recently developed and validated 358 consistent cortical landmarks, or regions of interests (ROIs), in [5], which provide intrinsic structural and functional correspondences across individuals and populations. Thus, the WQCPs from different temporal segments of multiple brains can be readily pooled and effectively compared via sparse coding and representation methods, which can learn the most descriptive atomic patterns in forming a meaningful dictionary to represent and discriminate those WQCPs. Our experimental results demonstrated that the learned ACPs for R-fMRI and T-fMRI datasets are substantially different, as expected, but the overlapping ACPs suggest that certain subjects were not in the expected task-free/task-performance states and should be considered as outliers in the following steps of data analysis.

2 Materials and Methods

2.1 Overview

The flowchart of the proposed computational framework is summarized in Fig. 1. First, 358 cortical ROIs discovered and validated in our recent study in [5] are located in the brain using DTI data (green bubbles in the left panel of Fig. 1). Then, both resting state fMRI (R-fMRI) and visual-task fMRI (T-fMRI) time series for each ROI are extracted. By using a sliding time window, the dynamic functional connectivity time series between each pair of ROIs are measured and the cumulative connectivity

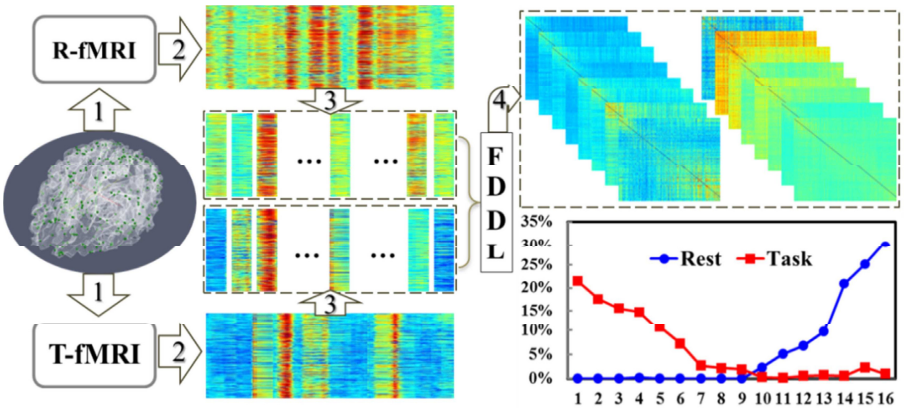

Fig. 1. The flowchart of our computational framework. (1) fMRI signal extraction for each ROI; (2) Measurement of dynamic functional connectivity strength; (3) Manual segmentation and collection of WQCP training samples; (4) FDDL sparse learning and classification.

strength of each ROI at each time point is summed. It is observed that the functional connectivity strengths are relatively stable in a continuous time period, and then the dynamic functional connectivity time series are manually segmented into quasi-stable time periods (called WQCP above), which form a set of WQCP training samples. Finally, the WQCP samples from both R-fMRI and T-fMRI datasets were combined together for sparse representation learning via the Fisher discriminative dictionary learning (FDDL) method [4].

2.2 Data Acquisition and Pre-processing

Twenty-six healthy adolescent volunteers participated in this study under IRB approvals. Multimodal DTI and fMRI datasets were acquired on a 3T GE MRI scanner. Both resting state fMRI and block-based visual task fMRI scans were acquired for each volunteer. Acquisition parameters for the scans were as follows. fMRI: 64×64 matrix, 4mm slice thickness, 220mm FOV, 30 slices, TR=2s; Visual task design and imaging parameters are referred to our recent publication [7]. DTI: 256×256 matrix, 3mm slice thickness, 240mm FOV, 50 slices, 15 DWI volumes, b-value=1000. The pre-processing of the DTI data included brain skull removal and motion correction. Both resting state and visual task-based fMRI datasets were pre-processed using the FSL FEAT.

2.3 WQCP Extraction

Based on the DTI data of each subject, we predicted the 358 cortical landmarks via the functional ROI prediction approaches in [5]. In brief, these 358 cortical landmarks were optimized to possess consistent group-wise structural connection patterns, and thus have structural and functional correspondences across individuals and populations. The left panel of Fig.1 shows an example of the distributions of the 358 cortical landmarks on a cortical surface. In particular, these 358 cortical landmarks

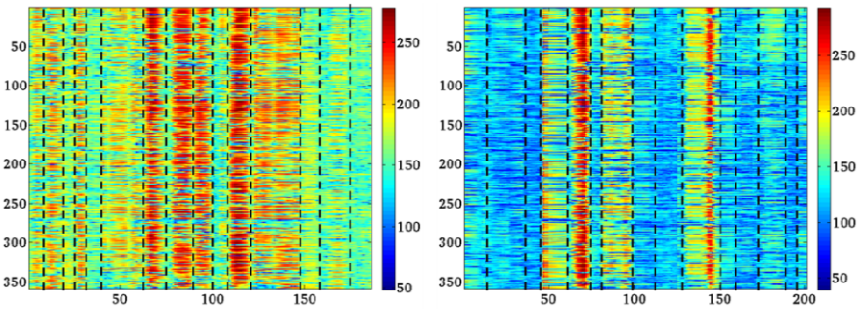

Fig. 2. The dynamic functional connectivity strength time series and WQCP segments. The horizontal axis represents time points and the vertical axis represents the cumulative functional connectivity strength of each ROI. The WQCPs are marked by the dash black lines. (a) A resting state fMRI case; (b) A visual task fMRI case.

are reproducible and predictable across different brains and most of them have been functionally annotated into meaningful networks via either benchmark task-based fMRI data or functional meta-analysis [5, 6]. Thus, this set of 358 cortical landmarks offers a common and individualized brain reference system for functional connectivity analysis, which is also adopted here in this paper.

After all the 358 cortical landmarks were located in the subject's brain, the fMRI time series for each landmark can be extracted from R-fMRI and T-fMRI datasets (Section 2.2). To investigate the temporally dynamics of the large-scale functional brain connectivities, a sliding time window approach was applied here. At each time point *t*, the functional connectivity between each pair of ROIs (*i* and *j*) is defined by:

$$FC_{i,j} = abs\left(Pearson\ Correlation\left(W_i, W_j\right)\right),\ FC_{i,j} = 0, \text{if } i = j; \tag{1}$$

where $W_i = [s_{i,t}, s_{i,t+1}, \ldots, s_{i,t+l-1}]$ and $W_j = [s_{j,t}, s_{j,t+1}, \ldots, s_{j,t+l-1}]$. l is the length of the time window; $s_{i,t}$ and $s_{j,t}$ are the fMRI signal strengths of ROI *i* and ROI *j* at the time point *t*. FC is measured using the absolute value of Pearson correlation coefficient between the two *l*-time-points length fMRI time series W_i and W_j. After the dynamic functional connectivity time series between each pair of ROIs are obtained, the cumulative connectivity strength of each ROI is measured by summing all the functional connectivities between this ROI and all of the other ROIs. This converts the functional connectivity matrix into a representative connectivity vector at each time point. Then, we obtained a 2D dynamic functional connectivity strength matrix for each participant (see Fig. 2). In this figure, the horizontal axis represents time points and the vertical axis is the cumulative functional connectivity strength of each ROI, which is color-coded by the color-bar on the right. From Fig. 2, it can be observed that the connectivity strength keeps relatively stable in a continuous time period. Therefore, the dynamic connectivity matrix is manually segmented into a series of shorter time segments, called whole-brain quasi-stable connectivity patterns (WQCP). Then, since the functional connectivity pattern within each WQCP is quasi-

stable, each WQCP segment is averaged among the time axis, resulting in a single WQCP vector. Two experts performed segmentation work and independently checked. Finally we obtained a collection of 1149 consistent WQCP vectors from the datasets in Section 2.2. Specifically, there are 474 WQCP vectors for resting state data and 675 WQCP vectors for visual task data. All these WQCP segments and vectors were pooled together as training samples and represented using the following methods.

2.4 FDDL for Sparse Representation of WQCP

Sparse representation has been widely demonstrated to exhibit very good performance in a variety of image analysis applications such as image classification [4, 9]. Typically, there are two steps in the sparse representation based image classification method: coding and classification. In sparse representation, learning the descriptive and representative dictionary is the key. Sparse dictionary learning has been used in the brain activity and function study [11]. This paper adopted the recently developed Fisher discriminative dictionary learning (FDDL) based sparse representation methodology [4] and tailored it for our functional brain state learning applications.

Briefly, the FDDL method employs a Fisher discrimination criterion to learn a structured dictionary, based on which the classification is performed. Here, the learned dictionary is denoted by $D = [D_1, D_2, \dots, D_c]$, where D_i is the sub-dictionary corresponding to the class i, and c is the total number of classes learned. Also, $A = [A_1, A_2, \dots, A_c]$ represents the training WQCP vector samples, where A_i is the sub-set of the training WQCP vector samples belonging to the class i. In addition, $X = [X_1, X_2, \dots, X_c]$ represents the coding coefficient matrix of A over D. The FDDL model is represented as follows:

$$J_{(D,X)} = argmin_{(D,X)}\{r(A, D, X) + \lambda_1\|X\|_1 + \lambda_2 f(X)\} \quad (2)$$

where the first term on the right $r(A, D, X)$ is called the discriminative fidelity term; the second term $\|X\|_1$ is the sparsity constraint; and the last term $f(X)$ is a Fisher discrimination constraint imposed on the coefficient matrix. λ_1 and λ_2 are scalar parameters for trade-off between sparsity and discrimination capability. Here, λ_1=0.005 and λ_2=0.05.

Specifically, there are two classifiers that can be used: global classifier (GC) and local classifier (LC) [4]. This study adopted the GC to perform the sparse coding learning and classification. For one input WQCP vector sample y, first, the sparse coding coefficients can be obtained by solving the following:

$$\hat{\alpha} = argmin_{\alpha}\{\|y - D\alpha\|_2^2 + \gamma\|\alpha\|_1\} \quad (3)$$

where $\hat{\alpha} = [\hat{\alpha}_1; \hat{\alpha}_2; \dots; \hat{\alpha}_c]$ and $\hat{\alpha}_i$ is the coefficient vector linked to the D_i. γ is a constant parameter. Then, the sample y is attributed to the class, associated with which the sub-dictionary has the minimum representation error defined by Eq. 4:

$$e_i = \|y - D_i\hat{\alpha}_i\|_2^2 + w \cdot \|\hat{\alpha} - m_i\|_2^2 \quad (4)$$

where the first term is the reconstruction error using class i, and the second term is the distance between $\hat{\alpha}$ and m_i. m_i is the learned mean vector and w is a constant.

This study used and tailored the above FDDL methodology to train the pooled resting state and task-based WQCP vector samples to achieve a compact and meaningful dictionary. In particular, each sub-dictionary or class is associated with an atomic connectivity pattern (ACP), and here the total number of ACPs (and thus sub-dictionaries) is set to be 16, which is optimally selected based on many experiments. Afterward, we used the GC to classify the WQCP samples into 16 ACP patterns and obtained the distributions of WQCP vectors for both resting state and task samples in each ACP. Finally, each ACP pattern is described and represented by the averaged center of all of the WQCP segments and WQCP vectors belonging to this pattern.

3 Experimental Results

3.1 Distributions of 16 ACPs in R-fMRI and T-fMRI Datasets

Using methods in Sections 2.4, we obtained a combined dictionary containing 16 sub-dictionaries or ACPs. Then, each WQCP sample is classified into one ACP in correspondence with one sub-dictionary. The distributions in the 16 ACPs for both task-free and task-performance WQCP samples are drawn in Fig. 3. The horizontal axis indexes the 16 ACPs discriminated by the FDDL dictionary. The vertical axis represents the percentages of WQCP samples distributed in each ACP for both task-free and task-performance datasets.

From Fig. 3, it can be observed that the task-free and task-performance periods show quite different distribution patterns. In total, there are 94.2% of task-performance WQCP samples distributed in ACPs #1~#9, which can be considered as the task-performance ACP patterns. Also, there are 97.5% task-free WQCP samples distributed in the ACPs #11~#16, which should be considered as task-free ACP patterns. However, for ACP #10 (highlighted by black arrow in Fig. 3), the task-free and task-performance WQCP samples overlap and the percentages for both are lower than 3%. Importantly, it is exactly these overlapped WQCP samples that imposed difficulty to decide which functional state (task-free or task-performance) it really belongs to, and we consider them as an uncertain pattern or even outliers in the other following steps of data analysis, such as identification of resting state networks (RSNs) and task-based functional region localization.

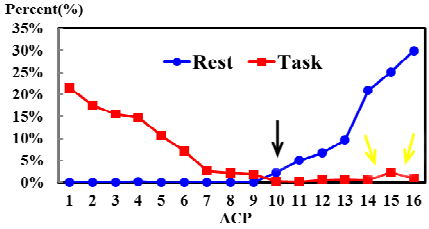

Fig. 3. The distributions of resting state and task-based WQCP samples in 16 ACP patterns

3.2 Visualization and Quantitative Analysis of ACPs

To explore more neuroscience meanings of the ACP patterns, we visualized these 16 ACPs using their averaged WQCP centers. In Fig. 4, each ACP pattern is represented by a 358×358 functional connectivity matrix corresponding to one WQCP center.

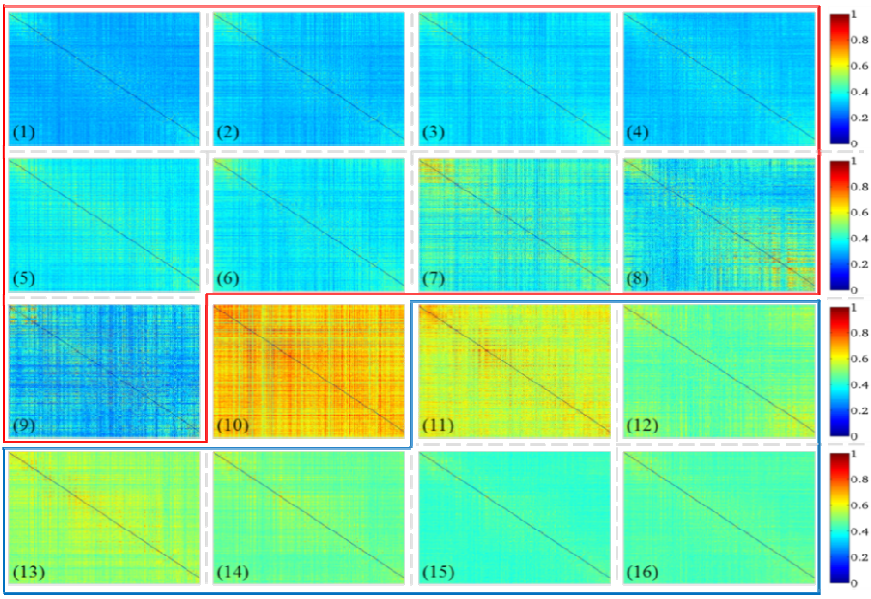

Fig. 4. Sixteen ACP patterns. It is a compact representation of task-free and task-performance states together.

In Fig. 4, ACPs #1~#9 (Fig. 3) are considered as task-performance ACP patterns (in the red frame in Fig. 4) and ACPs #11~#16 are considered to be task-free ACP patterns (in the blue frame in Fig. 4). It can be easily appreciated that ACP patterns in resting state and task-performance are quite different.

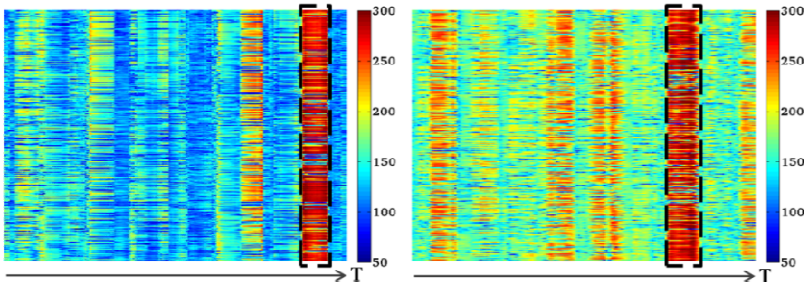

Fig. 5. WQCP samples with ACP pattern #10 in task-performance (left) and resting state (right). The ACP pattern #10 is highlighted by the dashed black box.

In total, we found 11 WQCP samples in 8 task-free subjects and 2 WQCP samples in 2 task-based subjects that were classified into the uncertain ACP #10. This pattern (Fig. 4(10)) exhibits quite high global functional connectivity, and Fig. 5 shows two examples from both T-fMRI and R-fMRI WQCP samples. In addition to the shared ACP #10 in Figs.3-4, we further investigated the potential outliers in both resting state and task-performance WQCP samples. For instance, there is one WQCP sample in a task-free subject, but it was clustered into the ACP #4, which is considered as one task-performance ACP. Importantly, we found 37 WQCP segments (out of totally 675 task-performance WQCP samples) in 17 subjects that were clustered into the task-free ACPs, as shown by the red boxes in the right side of Fig. 3 (highlighted by the yellow arrows). The quantitative summaries are provided in Table 1. These results imply that the participants in our experiments exhibited relatively good resting performance for high quality R-fMRI data, but they did not perform equally well in visual task experiments, as 17 of them exhibited resting state ACP patterns during the task-performance scans, suggesting these subjects were not well following the administered tasks in certain periods. Thus, we should take additional caution when analyzing the task-based fMRI datasets of these 17 subjects.

Table 1. The numbers and percentages of subjects with detected outlier ACP patterns.

ACP	Rest	Task
	Num/Percent	Num/Percent
Pattern #1	0	-
Pattern #2	0	-
Pattern #3	0	-
Pattern #4	1/3.8%	-
Pattern #5	0	-
Pattern #6	0	-
Pattern #7	0	-
Pattern #8	0	-
Pattern #9	0	-
Pattern #10	8/30.8%	2/7.7%
Pattern# 11	-	1/3.8%
Pattern #12	-	4/15.4%
Pattern #13	-	4/15.4%
Pattern #14	-	3/11.5%
Pattern #15	-	11/42.3%
Pattern #16	-	3/11.5%

4 Discussion and Conclusion

This paper presents a novel framework for quantitative characterization of task-free and task-performance functional brain states via sparse representation of whole-brain quasi-stable connectivity patterns (WQCP). Experimental results have demonstrated that though the learned ACPs for R-fMRI and T-fMRI datasets are substantially different, a certain portion of overlapping ACPs between the two datasets suggests that some subjects were not in the expected task-free/task-performance states during R-fMRI/T-fMRI scan sessions. This result has important implications in detecting and controlling R-fMRI/T-fMRI data quality for other data analysis tasks. In the future, we will examine the detailed functional connectivity patterns in all ACPs. For instance, the ACP #16 in Fig. 4 can be clustered into several functional sub-networks (Fig. 6), and it turns out that the widely replicated default mode network [1] is within

one clustered sub-network, as highlighted by the red lines in Fig. 6. This result suggests that we can possibly define and cluster resting state networks, e.g., the ones within the black boxes in Fig. 6, within each temporally quasi-stable ACP pattern, in which the temporal patterns of functional connectivities are much more homogeneous and stable than those in traditional RSN identification methods that consider the entire R-fMRI scan period [2].

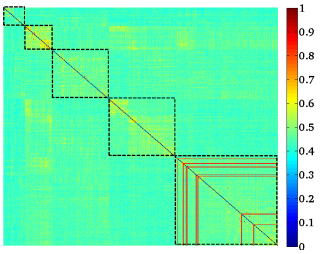

Fig. 6. The default mode network (DMN) in ACP pattern #16

References

1. Raichle, M.E., MacLeod, A.M., Snyder, A.Z., Powers, W.J., Gusnard, D.A., Shulman, G.L.: A default mode of brain function. Proc. Natl. Acad. Sci. USA 98(2), 676–682 (2001)
2. Fox, M.D., Raichle, M.E.: Spontaneous fluctuations in brain activity observed with functional magnetic resonance imaging. Nat. Rev. Neurosci. 8, 700–711 (2007)
3. Heeger, D.J., Ress, D.: What does fMRI tell us about neuronal activity? Nat. Rev. Neurosci. 3(2), 142–152 (2002)
4. Yang, M., Zhang, L., Feng, X., Zhang, D.: Fisher Discrimination Dictionary Learning for Sparse Representation. In: ICCV, Barcelona, pp. 543–550 (2011)
5. Zhu, D., Li, K., Guo, L., Jiang, X., Zhang, T., Zhang, D., Chen, H., Deng, F., Faraco, C., Jin, C., Wee, C.Y., Yuan, Y., Lv, P., Yin, Y., Hu, X., Duan, L., Hu., X., Han, J., Wang, L., Shen, D., Miler, L.S., Li, L., Liu, T.: DICCCOL: Dense Individualized and Common Connectivity-Based Cortical Landmarks. Cerebral Cortex (accepted, 2012)
6. Laird, A.R., Eickhoff, S.B., Kurth, F., Fox, P.M., Uecker, A.M., Turner, J.A., Robinson, J.L., Lancaster, J.L., Fox, P.T.: ALE meta-analysis workflows via the BrainMap database: Progress towards a probabilistic functional brain atlas. Front Neuroinformatics 3(23) (2009)
7. Zhang, T., Guo, L., Li, K., Jin, C., Hu, X., Cui, G., Li, L., Liu, T., Li, L., Liu, T.: Predicting functional cortical ROIs via DTI-derived fiber shape models, Cerebral Cortex (2011) (in press)
8. FMRIB Software Library, `http://www.fmrib.ox.ac.uk/fsl/index.html`
9. Lee, H., Battle, A., Raina, R., Ng, A.Y.: Efficient sparse coding algorithms. In: Advances in Neural Informattion Processing Systems (NIPS), Vancouver, vol. 19, pp. 801–808 (2007)
10. Epstein, J.N., Casey, B.J., Tonev, S.T., Davidson, M., Reiss, A.L., Garrett, A., Hinshaw, S.P., Greenhill, L.L., Vitolo, A., Kotler, L.A., Jarrett, M.A., Spicer, J.: Assessment and prevention of head motion during imaging of patients with attention deficit hyperactivity disorder. Psychiatry Res. 155(1), 75–82 (2007)
11. Varoquaux, G., Gramfort, A., Pedregosa, F., Michel, V., Thirion, B.: Multi-subject dictionary learning to segment an atlas of brain spontaneous activity. Inf. Process Med. Imaging 22, 562–573 (2011)